Extended Finite Element Method for Calculation of Eddy Currents at High Frequencies

Shingo Hiruma, *Member, IEEE*

Graduate School of Engineering, Kyoto University, Kyoto, 615-8510, Japan

The extended finite element method is used for calculating eddy currents at high frequencies, which reduces the number of unknowns in conductive materials. In this study, 2D and 3D models are analyzed numerically, and the solutions are compared with the solution obtained using the conventional finite element method. The proposed method is shown to give the accurate eddy current distribution and Joule losses for a wide range of frequencies even when the skin depth is smaller than the size of elements in a mesh.

***Index Terms*—eddy currents, extended finite element method, skin effect, surface impedance boundary condition.**

I. Introduction

THE evaluation of eddy currents is important for reducing the losses in electrical machines. The use of the finite element method (FEM), however, can be computationally expensive for eddy current problems with high skin effect because the size of the finite element needs to be smaller than the skin depth.

To reduce the computational cost, the surface impedance boundary condition (SIBC) [1], homogenization methods [2], [3] and model-order reduction techniques [4] have been studied. Despite their successful application in eddy current problems, each method has its disadvantages. For example, in SIBC, the accuracy decreases at low frequencies and the normal component of the magnetic field at the surface of the conductor cannot be considered.

In this paper, we propose an alternative solution to reduce the computational cost using the extended FEM (XFEM) [5]-[7]. In this formulation, a new enrichment function is used for eddy current problems. The proposed method can be used for a wide range of frequencies with a low cost of mesh generation and requires only a few hypotheses on the eddy current distribution. To validate the proposed method, 2D and 3D eddy current problems are solved using the proposed XFEM, and the solutions are compared with the numerical solutions obtained using the conventional FEM (CFEM).

II. Method

A. Principle of extended finite element method

XFEM is an extension of CFEM, which is designed to treat discontinuities without mesh refinement. To achieve this, enrichment functions that reflect domain information, such as discontinuities and solution characteristics, are used to extend the solution space. In XFEM, the XFE approximation of a scalar function $u(\boldsymbol{x})$ is expressed as [5] follows:

Manuscript received April 1, 2015; revised May 15, 2015 and June 1, 2015; accepted July 1, 2015. Date of publication July 10, 2015; date of current version July 31, 2015. (Dates will be inserted by IEEE; "published" is the date the accepted preprint is posted on IEEE Xplore®; "current version" is the date the typeset version is posted on Xplore®). Corresponding author: Shingo Hiruma (e-mail: hiruma.shingo.3w@kyoto-u.ac.jp).

$$u_h(\boldsymbol{x}) = \sum_{i\in I} u_i N_i(\boldsymbol{x}) + \sum_{i\in E} N_i(\boldsymbol{x}) \left(\sum_j \psi_j(\boldsymbol{x}) a_{ij} \right) \quad (1)$$

where $N_i(\boldsymbol{x})$ is the ith shape function, which is equivalent to that used in CFEM; u_i, a_{ij} are unknowns at the ith node; $\psi_j(\boldsymbol{x})$ is the jth enrichment function; and I, E are the set of nodes in the domain and the enriched nodes, respectively. The functions $N_i(\boldsymbol{x})\psi_j(\boldsymbol{x})$ can be regarded as enriched shape functions that extend the solution space.

As discussed in [7], the XFE approximation of a vector-valued function $\boldsymbol{A}(\boldsymbol{x})$ is introduced as follows:

$$\boldsymbol{A}_h(\boldsymbol{x}) = \sum_{i\in I} A_i \boldsymbol{w}_i(\boldsymbol{x}) + \sum_{i\in E} \boldsymbol{w}_i(\boldsymbol{x}) \left(\sum_j \psi_j(\boldsymbol{x}) A_{ij} \right) \quad (2)$$

where $\boldsymbol{w}_i(\boldsymbol{x})$ is the edge element of the ith edge; A_i, A_{ij} are the unknowns of the ith edge; and I, E are the sets of edges in the domain and the enriched edges, respectively. Equation (2) is applied to the 3D eddy current problems where the magnetic vector potential is discretized using the edge element.

B. Choice of enrichment function for eddy current problems

XFEM was originally proposed to analyze crack propagation, for which Heaviside functions and Westergaard solutions were used as enrichment functions to treat discontinuities in the analysis domain and stress singularities at the crack tips, respectively [5]. XFEM is also used to analyze the Helmholtz equation, for which plane waves are used as enrichment functions [6]. The choice of enrichment function is significant for appropriately expanding the solution space. In this section, we discuss the *a priori* knowledge of eddy current behavior in choosing the enrichment function.

At high frequencies, the current density is concentrated near the surface of the conductor owing to the skin effect and its magnitude decreases exponentially moving away from the surface. When the skin depth δ is smaller than the curvature and characteristic length of the conductor, the tangential component of the electric field $E_{\parallel}$ in the conductor is governed by the Helmholtz equation [8]:

$$\frac{\mathrm{d}^2 E_{\parallel}(\xi)}{\mathrm{d}\xi^2} - \mathrm{j}\omega\sigma\mu E_{\parallel}(\xi) = 0, \qquad 0 \le \xi \tag{3}$$

where $\xi, j, \omega,$ and μ are the local coordinates equivalent to the distance from the surface of the conductor, imaginary unit, angular frequency, and permeability, respectively. To reproduce this behavior on a local scale, we can use the general solution of the equation as an enrichment function as follows:

$$\psi(\boldsymbol{x}) = \exp\big(-\gamma\xi(\boldsymbol{x})\big) \tag{4}$$

where $\gamma = \sqrt{j\omega\sigma\mu}$. The geometric variables and local coordinate system are depicted in Fig. 1 (a).

The enrichment function (4) expands the solution space of the tangential component of the electric field and current density at high frequencies, whereas the normal component of such quantities is represented by the conventional FE approximation. Considering the normal component of the magnetic field at the surface of the conductor in SIBC, which approximates only the tangential component, is difficult.

C. *Choice of enriched nodes and edges*

In the 2D and 3D analyses, the nodes and edges enriched using the enrichment function are chosen near the surface of the conductor to consider the skin effect. In the 3D analysis, we additionally use *a priori* knowledge to choose the set of enriched edges. As stated in Section II-B, the tangential component of the solution space is expanded using the enrichment function. Therefore, we choose enriched edges that are parallel to the surface of the conductor. To this end, hexahedral elements depicted in Fig. 1 (b) are used.

D. *Computation of FE matrix*

The Galerkin method is used to derive the weak form of the governing equation. Let $\mathcal{V}_h^{\mathrm{FEM}}$ represent the test space used in CFEM. The test space $\mathcal{V}_h^{\mathrm{XFEM}}$ can be expressed as follows:

$$\mathcal{V}_h^{\mathrm{XFEM}} = \left\{ \sum_{i\in I} a_i \boldsymbol{w}_i + \sum_{i\in E} b_i \psi(\boldsymbol{x}) \boldsymbol{w}_i \,\middle|\, \begin{matrix} \boldsymbol{w}_i \in \mathcal{V}_h^{\mathrm{FEM}} \\ a_i, b_i \in \mathbb{C} \end{matrix} \right\} \tag{5}$$

In the 3D problem, the weak form of the eddy current problem using the A formulation is expressed as follows:

$$\begin{aligned} \int_\Omega \nabla\times\boldsymbol{w}^*\cdot\nu\nabla\times\boldsymbol{A}d\Omega + j\omega\int_\Omega \boldsymbol{w}^*\cdot\sigma\boldsymbol{A}d\Omega \\ = \int_\Omega \boldsymbol{w}^*\cdot\boldsymbol{J}_0 d\Omega, \qquad \forall\boldsymbol{w}\in\mathcal{V}_h^{\mathrm{XFEM}} \end{aligned} \tag{6}$$

where $*$ represents the complex conjugate operator and ν denotes the magnetic reluctivity. Owing to the conjugate operator, the second term on the left-hand side leads to a skew Hermitian matrix. Consequently, the coefficient matrix becomes nonsymmetric. In this study, we solve the XFE equation using an incomplete lower–upper (ILU) preconditioned bi-conjugate gradient stabilized (BiCGstab) method.

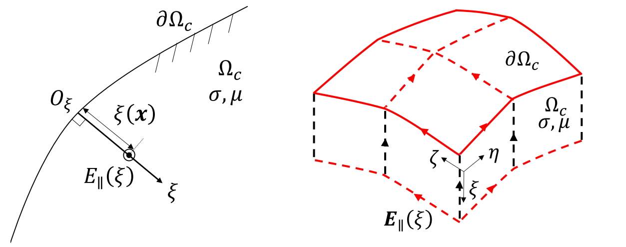

(a) (b)

Fig. 1. (a) One-dimensional local coordinate system near the surface of the conductor. The tangential component of the electric field $E_{\parallel}$ in the conductor is characterized by $\xi(\boldsymbol{x})$. (b) Hexahedral elements are used as enriched elements in 3D problem where the edges in red are enriched.

In the implementation of XFEM, the quadrature of the weak form is a significant issue because the approximation space is enriched using an exponential function. To address this issue, we used a higher-order Gaussian quadrature for the triangle and hexahedron [9].

E. *Low and high frequency limits*

At low frequencies, the value of the enrichment function over the enriched elements is $\psi(\boldsymbol{x}) \approx 1$. This implies that the enrichment term becomes almost equal to the standard FE approximation. Therefore, the solution of XFEM is equivalent to that of CFEM at the stationary limit.

At high frequencies, the current density concentrates near the surface of the conductor owing to the skin effect. Therefore, the second term of (2) is dominant. By letting (2) in $\boldsymbol{B} = \nabla\times\boldsymbol{A}$, the magnetic flux density can be approximated as:

$$\begin{aligned} \boldsymbol{B}(\boldsymbol{x}) &\approx \sum_{i\in E}\nabla\times\boldsymbol{w}_i(\boldsymbol{x})\psi(\boldsymbol{x})A_i \\ &\qquad + \sum_{i\in E}\nabla\psi(\boldsymbol{x})\times\boldsymbol{w}_i(\boldsymbol{x})A_i \\ &= \sum_{i\in E}\nabla\times\boldsymbol{w}_i(\boldsymbol{x})\psi(\boldsymbol{x})A_i \\ &\qquad - \gamma\sum_{i\in E}\psi(\boldsymbol{x})\nabla\xi(\boldsymbol{x})\times\boldsymbol{w}_i(\boldsymbol{x})A_i \\ &\approx -\gamma\nabla\xi(\boldsymbol{x})\times\boldsymbol{A} \end{aligned} \tag{7}$$

where the first term of the second line can be ignored because $|\gamma| \propto \sqrt{\omega}$ increases at high frequencies. The weak form in the conductive domain Ω_c, where $\boldsymbol{J}_0 = 0$, becomes

$$\begin{aligned} K_c &= \int_{\Omega_c}\nabla\times\boldsymbol{w}^*\cdot\boldsymbol{H}d\Omega + j\omega\int_{\Omega_c}\boldsymbol{w}^*\cdot\sigma\boldsymbol{A}d\Omega \\ &= \int_{\partial\Omega_c}\boldsymbol{w}^*\times\boldsymbol{H}\cdot\boldsymbol{n}d\Gamma \\ &\approx -\gamma\nu\int_{\partial\Omega_c}\boldsymbol{w}^*\times\big(\nabla\xi(\boldsymbol{x})\times\boldsymbol{A}\big)\cdot\boldsymbol{n}d\Gamma \\ &= \gamma\nu\int_{\partial\Omega_c}\boldsymbol{w}^*\cdot\big((\boldsymbol{n}\times\boldsymbol{A})\times\boldsymbol{n}\big)d\Gamma \end{aligned} \tag{8}$$

where the second line is obtained through integration by parts.

The last line is obtained based on $\nabla\xi(\boldsymbol{x}) = -\boldsymbol{n}$ at $\partial\Omega_c$, where $\boldsymbol{n}$ denotes the outward unit normal vector of the boundary. This is equivalent to the weak form of CFEM using SIBC [1]. Therefore, the solution of XFEM becomes equivalent to that of CFEM using SIBC at the high frequency limit.

III. Numerical Results

A. *Skin effect in cylindrical conductor*

Firstly, we consider a cylindrical conductor Ω of radius $r = 0.01$ m, conductivity $\sigma = 10^6$ S/m, and relative permeability $\mu_r = 1$. The domain Ω is bounded by Γ_D, where the Dirichlet boundary condition is imposed. The Cartesian coordinate system $(x,\ y,\ z)$ is introduced as illustrated in Fig. 2 (a). The uniform external current density $J_0\mathbf{e}_z$ is expressed in Ω. The z-component of the magnetic vector potential A_z is governed by

$$-\nabla\cdot\nu\nabla A_z(x,y) + \mathrm{j}\omega\sigma A_z(x,y) = J_0 \tag{9}$$

$$A_z(x,y) = 0, \qquad E_z(x,y) = 1 \quad \text{on } \Gamma_D \tag{10}$$

where $\nu = \mu^{-1}$. Based on the boundary conditions, we use $J_0 = \sigma$ in Ω.

We solved the CFE and XFE equations using the mesh illustrated in Fig. 2 (b), where the nodes indicated in the gray elements are enriched. We used the fifth-order Gaussian quadrature formula for a triangle to compute the elements in the matrices in the XFE equation. For comparison, we obtained a reference solution by solving the CFE equation using a fine mesh considering skin depth at the normalized frequency $r/\delta = 15$, where $\delta = \sqrt{2/\omega\sigma\mu}$. The numbers of DOFs are 37 in CFEM with the coarse mesh, 63 in XFEM, and 9,489 in CFEM with the fine mesh, respectively. The solutions at $r/\delta = 15$ are depicted in Fig. 3. Despite the small skin depth, the solution obtained using XFEM accurately approximates the reference solution, whereas the solution obtained using CFEM with the coarse mesh is no longer acceptable at this frequency. The Joule loss and energy densities are plotted against the normalized frequency, as presented in Fig. 4. The results obtained from XFEM are in good agreement with those of the reference solutions.

B. *Skin effect in 3D problem*

To validate the proposed method in a 3D problem, we consider a solenoidal conductor model of width $r = 0.01$ m, conductivity $\sigma = 10^6$ S/m, and relative permeability $\mu_r = 1$, as illustrated in Fig. 5 (a). The eddy current problem with the current continuity equation and boundary conditions using the $A - V$ formulation can be formulated as follows:

$$\nabla\times\nu\nabla\times\boldsymbol{A} + \mathrm{j}\omega\sigma\boldsymbol{A} + \sigma\nabla V = 0 \tag{11}$$

$$\nabla\cdot(\mathrm{j}\omega\sigma\boldsymbol{A} + \sigma\nabla V) = 0 \tag{12}$$

$$\boldsymbol{A}\times\boldsymbol{n} = \boldsymbol{0} \quad \text{on } \Gamma_D \tag{13}$$

$$\boldsymbol{H}\times\boldsymbol{n} = \boldsymbol{0}, \qquad \nabla V\cdot\boldsymbol{n} = 0 \ \text{ on } \Gamma_N \tag{14}$$

$$\boldsymbol{A}\times\boldsymbol{n} = \boldsymbol{0}, \qquad V = \pm 1 \quad \text{on } \Gamma_{\mathrm{in}}, \Gamma_{\mathrm{out}} \tag{15}$$

where Γ_D and Γ_N are the Dirichlet and Neumann boundaries, respectively, and electric potential are imposed at Γ_{in} and Γ_{out}.

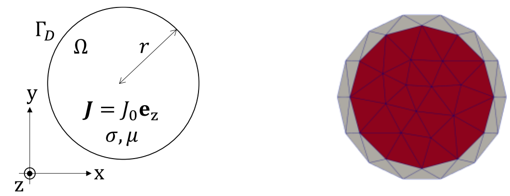

(a) (b)

Fig. 2. (a) Cylindrical conductor and (b) its discretization. The nodes indicated in the grey elements are enriched in XFEM.

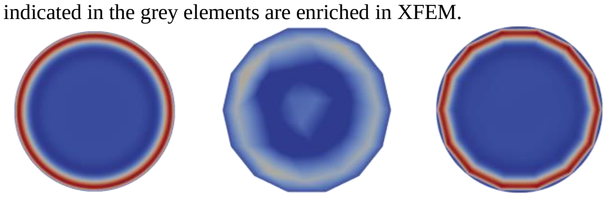

(a) (b) (c)

Fig. 3. Real part of vector potential obtained using (a) CFEM with fine mesh, (b) CFEM with mesh presented in Fig. 2, and (c) XFEM with mesh presented in Fig. 2 at normalized frequency $r/\delta = 15$.

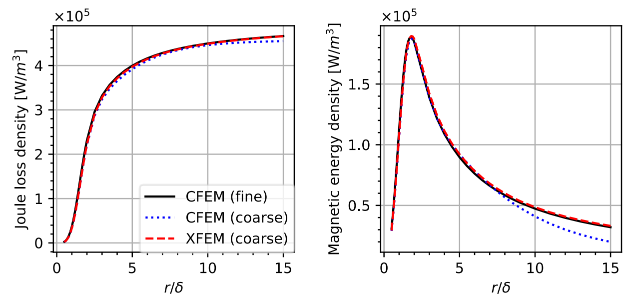

(a) (b)

Fig. 4. Frequency dependence of (a) Joule loss density and (b) energy density due to eddy currents in Ω obtained using CFEM and XFEM.

We solved the CFE and XFE equations with a coarse mesh illustrated in Fig. 5 (c), (d), where the edges in the blue elements are enriched. In XFEM, we used the enriched vector potential and standard electric scalar potential because the use of the enriched vector potential is suitable to express the eddy currents parallel to the surface of the conductor. We used the 10th-order Gaussian quadrature formula for a hexahedron. For comparison, we obtained a reference solution by solving the CFE equation using a fine tetrahedral mesh considering the skin depth at $r/\delta = 15$ as illustrated in Fig. 5 (b). The numbers of DOFs are 5,391 in CFEM with the coarse mesh, 6,047 in XFEM, and 2,377,300 in CFEM with the fine mesh, respectively. In Fig. 6, the Joule losses and their relative errors obtained from the reference solutions are plotted against the normalized frequency. The relative errors in XFEM are smaller than 3%, even though much less DOF are used in XFEM compared with CFEM using the fine mesh.

In XFEM, the equation was solved using the ILU-BiCGstab, whereas, in CFEM, it was solved using the incomplete Cholesky conjugate gradient solver. The iteration was stopped when the relative error became smaller than $\epsilon = 10^{-10}$. The number of iterations is plotted against the normalized frequency in Fig. 7 (a). We can see that XFEM requires more iterations when compared with the CFEM using the same mesh. This is because the XFE equation is nonsymmetric and the number of DOFs is larger than that in CFEM by the number of enriched edges. We can also see that the number of iterations in XFEM tends to increase at low frequencies. One possible reason for this is that the enrichment function approaches 1 at low frequencies; thus, the enrichment term would become redundant, which could result in ill-conditioned matrices.

The computational times required to obtain a solution using CFEM with the coarse and fine mesh and XFEM are compared in Fig. 7 (b). For this model, it took 5.10 and 27.0 s to build the CFE and XFE equations with the coarse mesh, respectively. The difference is caused by the higher-order Gaussian quadrature, which is required for numerical integration, including the exponential function. The computational time required to solve the XFE equation was 0.243 s, which was longer than 0.0483 s required in CFEM with the coarse mesh. This is attributed mainly to the increase in the number of DOFs and the difference in the matrix solver. Note that the total computational time in XFEM is still much smaller than that to obtain the reference solution.

IV. Discussion

To use the proposed method for practical applications such as the design of electric devices, we consider the following problems that must be addressed; (i) An efficient numerical or analytical quadrature formula is required to reduce the computational time required to construct the XFE equation; (ii) Ill-conditioning at low frequencies should be improved to reduce the number of iterations to solve the XFE equation; (iii) A method for time domain analysis is required to deal with the nonlinear material characteristics; (iv) The accuracy at the corner of the conductor, where the eddy currents get distributed in 2D or 3D, should be discussed; (v) An error analysis would be important to ensure the accuracy.

V. Conclusion

In this paper, we proposed an enrichment function for XFEM to deal with eddy current problems at high frequencies and with high skin effects. Since the coarse mesh can be used in XFEM, we can reduce the computational cost of the mesh generation and solving the FE equation. In future work, we will develop methods to solve the open problems discussed in Section IV.

Acknowledgment

This work was supported in part by the JSPS KAKENHI Grant Number 22K14237. We would like to thank Editage (www.editage.com) for their English language editing service.

References

[1] L. Krahenbuhl and D. Muller, “Thin Layers in Electrical Engineering. ¨ Example of Shell Models in Analysing Eddy-Currents by Boundary and Finite Element Methods,” *IEEE Trans. Magn.*, vol. 29, no. 2, pp. 1450–1455, March 1993.

[2] J. Gyselinck, P. Dular, N. Sadowski, P. Kuo-Peng and R. V. Sabariego, "Homogenization of Form-Wound Windings in Frequency and Time Domain Finite-Element Modeling of Electrical Machines," *IEEE Trans. Magn.*, vol. 46, no. 8, pp. 2852–2855, Aug. 2010.

[3] S. Hiruma and H. Igarashi, "Homogenization Method Based on Cauer Circuit via Unit Cell Approach," *IEEE Trans. Magn.*, vol. 56, no. 2, pp. 1–5, Feb. 2020.

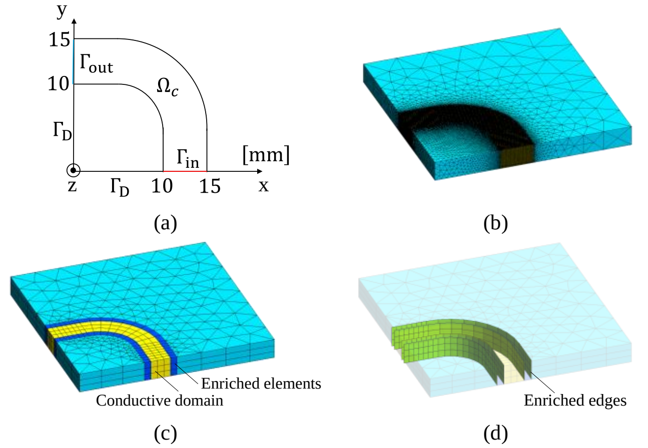

Fig. 5. (a) 3D solenoidal conductor model, (b) reference fine mesh, (c) coarse mesh, and (d) enriched edges in XFEM.

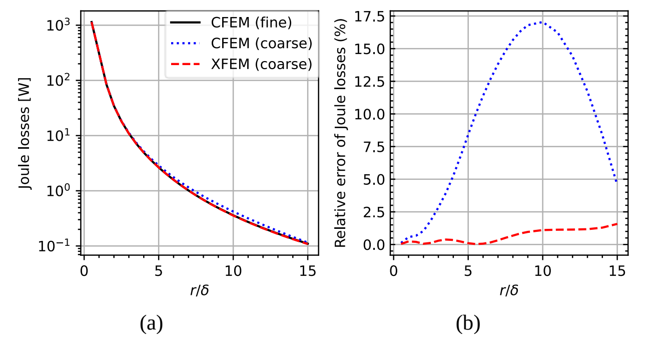

Fig. 6. (a) Joule losses plotted against normalized frequency and (b) its relative errors with respect to the reference solution using a fine tetrahedral mesh.

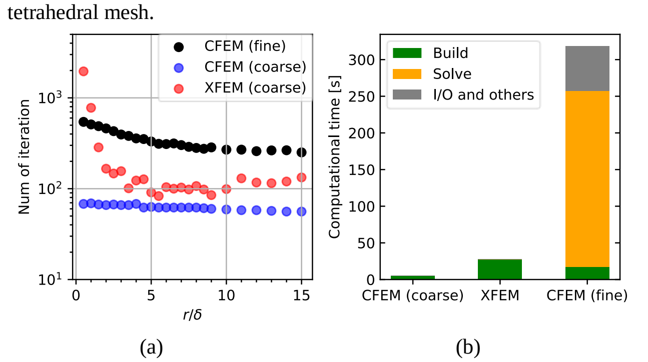

Fig. 7. (a) Number of iterations against normalized frequency for CFEM and XFEM using coarse mesh. (b) Computational time required to obtain a solution at the normalized frequency $r/\delta = 15$.

[4] K. Hollaus, J. Schöberl and M. Schöbinger, "MSFEM and MOR to Minimize the Computational Costs of Nonlinear Eddy-Current Problems in Laminated Iron Cores," *IEEE Trans. Magn.*, vol. 56, no. 2, pp. 1–4, Feb. 2020, Art. no. 7508104, doi: 10.1109/TMAG.2019.2954392.

[5] T. Belytschko, R. Gracie and G. Ventura, "A Review of Extended/Generalized Finite Element Methods for Material Modeling," *Model. Simul. Mater. Sci. Eng*., vol. 17, no. 4, pp. 043001, Apr. 2009.

[6] T. Strouboulis, I. Babuška and R. Hidajat, "The Generalized Finite Element Method for Helmholtz Equation: Theory Computation and Open Problems", *Comput. Methods Appl. Mech. Eng.*, vol. 195, no. 37, pp. 4711–4731, Jul. 2006.

[7] F. Lef`evre, S. Lohrengel and S. Nicaise, “An eXtended Finite Element Method for 2D Edge Elements,” *Int. J. Numer. Anal. Model.*, vol. 8, no. 4, pp. 641–666, 2011.

[8] J. D. Jackson, *Classical Electrodynamics (Third edition)*, Wiley (1999), pp. 352–356.

[9] Solin, Pavel, Karel Segeth, and Ivo Dolezel, *Higher-order Finite Element Methods*, Chapman and Hall/CRC (2003).